frontiers | Frontiers in Energy Research

TYPE Original Research
PUBLISHED 14 August 2024
DOI 10.3389/fenrg.2024.1441155

OPEN ACCESS

EDITED BY
Zhan Dou,
Beijing University of Chemical Technology, China

REVIEWED BY
Chi-Min Shu,
National Yunlin University of Science and Technology, Taiwan
Fahad Noor,
University of Engineering and Technology, Lahore, Pakistan

*CORRESPONDENCE
Xiaoliang Zhang,
yyyzxl@126.com

RECEIVED 30 May 2024
ACCEPTED 31 July 2024
PUBLISHED 14 August 2024

CITATION
Zhang X, Wang L, Tao G, Guo R, Fang J, Zhang J and Mao H (2024) Hydrogen production from aluminum-water reactions at low Temperatures: based on an *in-situ* two powders of different particle sizes.
Front. Energy Res. 12:1441155.
doi: 10.3389/fenrg.2024.1441155

Hydrogen production from aluminum-water reactions at low Temperatures: based on an *in-situ* two powders of different particle sizes

Xiaoliang Zhang*, Li Wang, Guangyuan Tao, Ronghan Guo, Jiawei Fang, Jun Zhang and Haifang Mao

Department of Safety Engineering, Shanghai Institute of Technology, Shanghai, China

To investigate the granule reaction of two-micron aluminum powders with water at low temperatures, differential scanning calorimetry was used to analyze the initial exothermic temperature. Additionally, adiabatic accelerated calorimetry was employed to study the exothermic reaction under adiabatic conditions. The hydrogen production and particle size variation were investigated in order to gain insights into the Al-water reaction in a reactor with no induction time. Through focused beam reflectance measurement analysis, it was observed that during the reaction process of Al-water, particle sizes initially increased and then decreased. Specifically, the particle size of 3 μm aluminum powder experienced a 189% increase after the reaction while 25 μm aluminum powder decreased by 29%. Ultimately, both types of particles reached similar final sizes around 13.89 μm. The process of Al-water reaction was explained and hydrogen production was analyzed, and the kinetic model was obtained.

KEYWORDS

Al-water reaction, exothermic reaction, FBRM analysis, reaction kinetics, hydrogen

1 Introduction

Nowadays, the pursuit of novel and effective hydrogen sources poses a formidable obstacle in the realm of hydrogen energy research, impeding its advancement in contemporary times (DAS, 1996). The decomposition of water for hydrogen production is widely regarded as an optimal approach (Ilyukhina et al., 2017). While many metals have the ability to split water into hydrogen and metal hydroxides, researchers have studied the reaction of metals such as Al (Soler et al., 2009; Tekade et al., 2018; Brayek et al., 2019), Mg (Zhang et al., 2019; Li et al., 2021; Chawla et al., 2022), Zn (Chen et al., 2022; Wei et al., 2022), and alloys (Xiao et al., 2019; Aman and Pradhan, 2022; Zhang Y. et al., 2022; Zhang Y. Y. et al., 2022) with water, among which, aluminum, has the advantages of high energy density, low price, environmentally safe reaction products, easy storage, and transportation, and is the most effective metal for splitting water (1.24L H_2 in 1 g of aluminum), which is considered one of the promising elements (Chen and Zhu, 2008; Chen et al., 2014; Razavi-Tousi and Szpunar, 2014; Godart et al., 2019; Chen et al., 2020; Fu et al., 2020; Trowell et al., 2020; Yu et al., 2022).

Aluminum reacts with water to form hydrogen, hydroxide or aluminum oxide, as shown in Table 1:

TABLE 1 Aluminum water chemical reactions (Ilyukhina et al., 2017; Dong et al., 2019; Bolt et al., 2020).

No.	Chemical equation
1	$3Al+2H_2O \rightarrow 2AlO + AlH_3+H$
2	$2AlO + H_2O \rightarrow Al_2O_3+H_2$
3	$2AlH_3 + 3H_2O \rightarrow Al_2O_3 + 6H_2$
4	$2Al+3H_2O \rightarrow Al_2O_3+3H_2$
5	$4Al + Al_2O_3 \rightarrow 3Al_2O$
6	$2Al+4H_2O \rightarrow 2AlOOH+3H_2$
7	$2Al+6H_2O \rightarrow 2Al(OH)_3+3H_2$
8	$Al(OH)_3+3Al \rightarrow 3AlO + AlH_3$
9	$Al(OH)_3+ AlH_3 \rightarrow Al_2O_3+3H_2$

In addition, metastable $[Al(H_2O)_6^{3+}]^*$ cluster ions can be produced by Al-water reaction under ambient condition, which can be as direct catalyst to decompose H_2O_2 into HO• radicals in a pH range from 2.5 to 12.0 (Guo et al., 2024).

Aluminum powder is easily oxidized at room temperature, resulting in the formation of a thin and dense oxide film on the surface (Wang et al., 2021). The existence of this oxide film makes it difficult for aluminum to react with water at room temperature (Tan et al., 2022). In order to solve this problem, the commonly used methods are ball milling of aluminum powder (Shkolnikov et al., 2011; Huang et al., 2013), adding alloy (Parmuzina and Kravchenko, 2008; Alinejad and Mahmoodi, 2009; Ziebarth et al., 2011), acid (Kumar and Muthukumar, 2020) or alkali (El-Meligi, 2011; Ambaryan et al., 2016; Milani et al., 2020; Tang et al., 2022) to the reaction, ultrasound induction (Huang et al., 2023) *etc.* The Al-water reaction temperature increases from 65°C to 85°C, the hydrogen production rate increases from 3.5 mL•min^{-1}•g•Al to 5.5 mL•min^{-1}•g•Al, and the conversion rate increases from 0.65 to 0.8 (Guo et al., 2024). Due to the limitations imposed by high temperatures on the application scenarios of Al-water reaction for hydrogen production, which not only consumes a substantial amount of energy but also entails certain risks, it becomes imperative to investigate the Al-water reaction at lower temperatures. The experiments conducted at elevated temperatures have indicated that the remarkable reactivity of aluminum powder may potentially trigger thermal runaway (Dong et al., 2019). Therefore, a comprehensive study on the Al-water reaction under low-temperature conditions is warranted.

At present, the research on the reaction mechanism of the Al-water system mainly uses the gas measurement method or calorimetry as experimental techniques. By obtaining data such as volume and generation rate of gas products (hydrogen) and heat release rate of the reaction, a reaction kinetic model is established. The form and parameters of this kinetic model are then used in combination to infer the reaction mechanism accurately. Saceleanu et al. (Saceleanu et al., 2019) used isothermal and non-isothermal calorimetry to determine the rate-determining step and corresponding activation energy of the reaction mechanism and found that there are two consecutive reaction stages in the micro/nano aluminum powder-liquid water reaction, namely, the JMAK nucleation-growth model in the first stage and the constant nuclear growth power law model in the second stage. Xinyang Wang et al. (Guo et al., 2024) observed the morphological development of hydroxide products through a series of isothermal experiments and proposed a multi-stage analysis model. In addition, Larichev Mikhail Nikolaevich (Nikolaevich et al., 2014) proposed a different hydrogen water reaction process through the hydrogen evolution rate of the near-room temperature aluminum molten reaction. However, the above studies did not pay attention to the online growth and change of particle surface structure during the reaction, which is helpful to the study of the Al-water reaction mechanism.

Due to the low ignition temperature and potential for explosion of nano-Al (Jiang et al., 2021), this paper focuses on micron aluminum powder as the subject of investigation. In this paper, the Al-water reaction process was studied experimentally and theoretically. By utilizing DSC and ARC observations, the initial exothermic temperature of the Al-water reaction is determined, providing valuable data into the temperature conditions associated with this reaction. The process of hydrogen production from the Al-water heterogeneous reaction was studied in agitated at low temperature of 45°C–85°C, because there will be a long induction time for the Al-water reaction without stirring (Gai et al., 2012), by measuring its hydrogen evolution and hydrogen generation rate, monitoring the particle size change and morphological change of process products during the Al-water reaction process to illustrate the mechanism of Al-water reaction.

2 Materials and methods

2.1 Materials

Two sizes of aluminum powder were used in the experiment, sample 1 was 3 μm and sample 2 was 25 μm, aluminum content of not less than 99.95%, both purchased from Shanghai Titan Technology Co., Ltd. Figure 1 shows the particle size distribution of two kinds of aluminum powder by Bettersize2600. Water used in the experiment is pure water.

2.2 Exothermic properties of the Al-water reaction

DSC and ARC were used to study the exothermic properties of the Al-water reaction, as shown in Figure 2A. The Al-water reaction was studied via DSC using a differential calorimeter (NETZSCH, Germany) to investigate its thermodynamic behavior in a high-pressure stainless steel crucible. In the DSC experiment, the mass of aluminum powder was 3 mg ± 0.2, the mass of water was 6 mg ± 0.2, and the thermodynamic parameters such as initial exothermic temperature, peak temperature were determined at the heating rates of 5, 7.5, and 10 K/min, and the temperature range was from 30°C–200°C. ARC (Thermal Hazard Technology, United Kingdom) was used to study the heat release of the Al-water reaction in a titanium alloy sample ball under adiabatic conditions. In the ARC experiment, the mass of aluminum powder was 0.05 mg, the mass of water was 0.1 mg, choose heat-wait-search mode, and the temperature range was from 30°C–200°C.

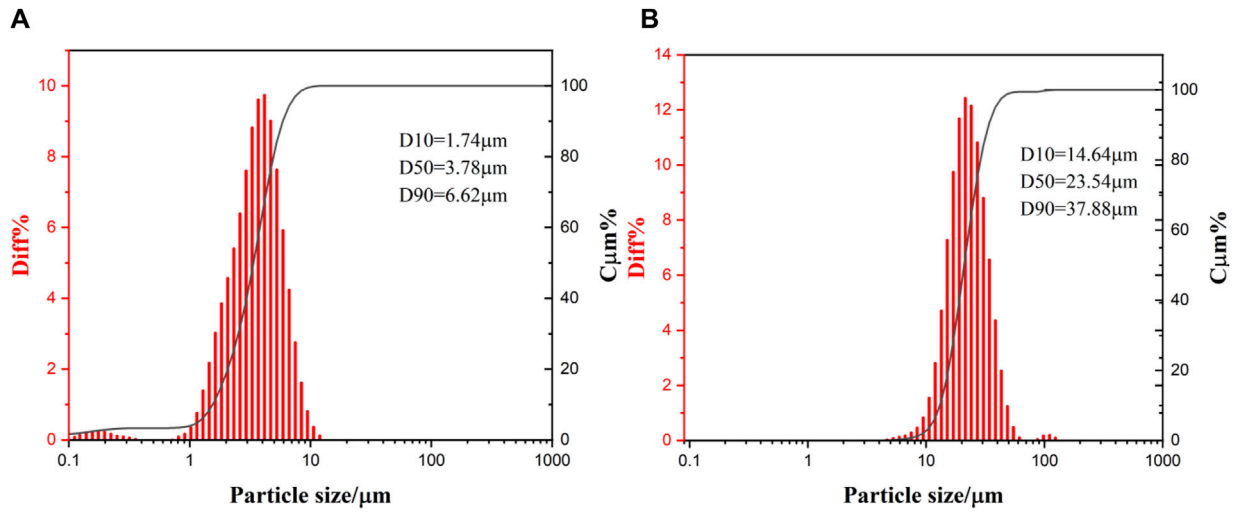

FIGURE 1
(A, B) Particle size distribution diagram of two particle sizes of aluminum powder.

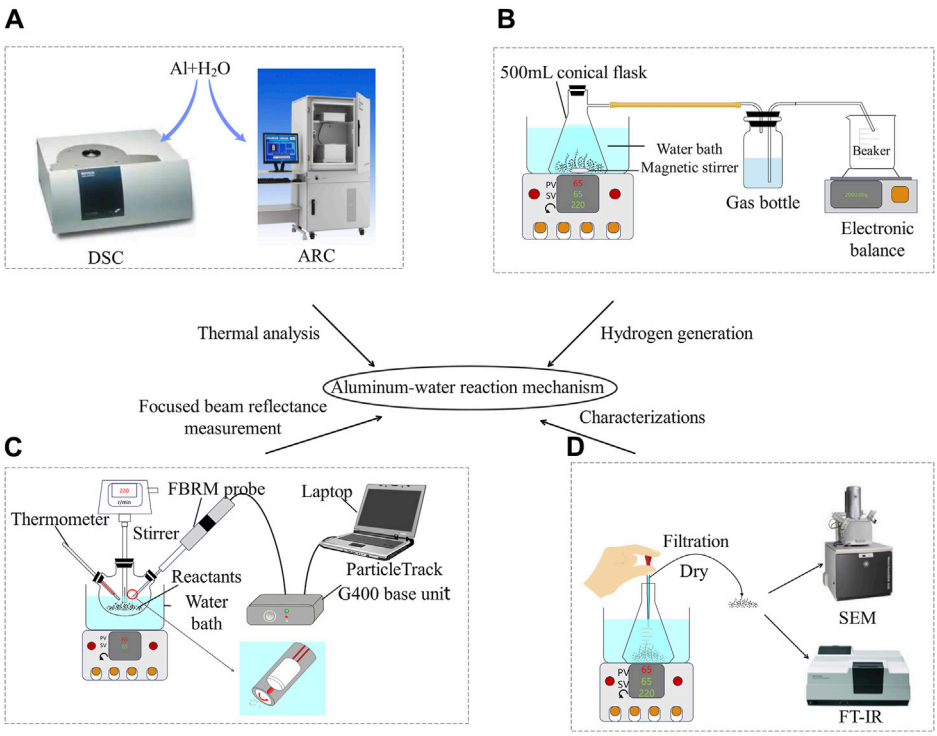

FIGURE 2
(A–D) Schematic diagram of the Al-water reaction experiment.

2.3 Hydrogen production by Al-water reaction experiments

A series of isothermal experiments were performed to measure the amount and rate of hydrogen production from the Al-water reaction. The experiment was performed at 45°C–85°C, because this series of temperatures is easy to reach and more energy-efficient in production, the device diagram is shown in Figure 2B, and the evolution and rate of the generated hydrogen was indirectly measured by the drainage method, by reading the data from the electronic balance can know the mass and volume of the discharged water, and then the volume of the gas generated by the reaction. Before the experiment, the hydrogen collection cylinder is filled with enough water and plugged with a stopper with a delivery pipe, in

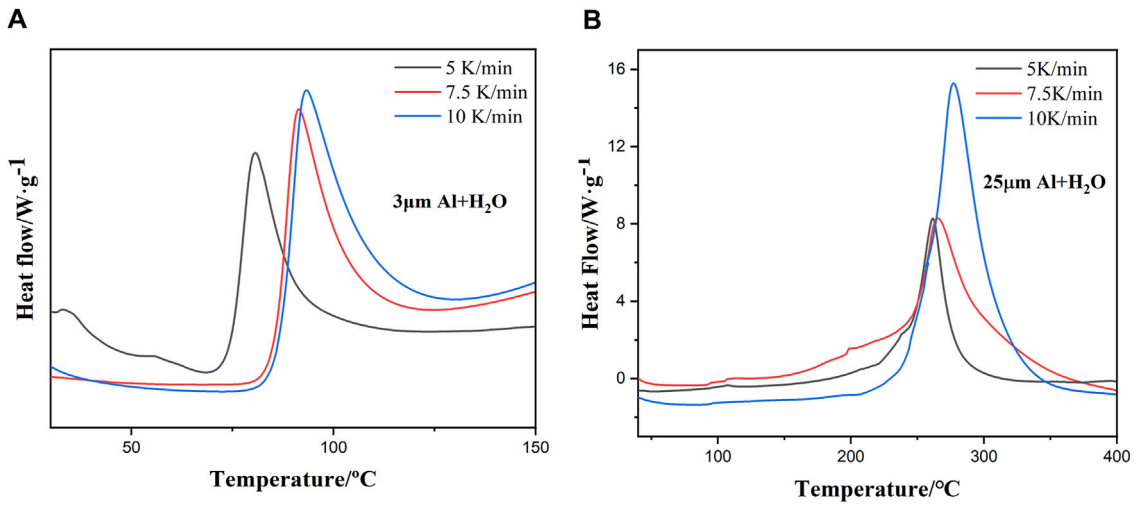

FIGURE 3
(A, B) Heat flow curves of the Al-water reaction with different ratios under three different heating.

which an empty beaker placed on the electronic balance is inserted at the other end of the long tube of the stopper to collect and measure the discharged water (the electronic balance is zeroed before the experiment, and the hydrogen is compressed because it is collected at room temperature), and the other end of the short tube of the stopper is connected to a flask that the Al-water reaction to transport hydrogen. Put a rotor in the flask and add 200 mL of pure water, put the flask with water into the water bath. After that, start heating, and when the temperature reaches the set temperature, add 0.5 g of aluminum powder and immediately open the stirring (220r/min) and plug the plug, stirring was used to speed up the Al-water reaction and shorten the induction time. The reaction time and displacement are recorded at the same time.

2.4 Focused beam reflectance measurement

To monitor the distribution of particle chord lengths during the aluminum powder reaction, the analysis was performed with a FBRM probe (METTLER, G400), shown in Figure 2C, which is inserted into the fluid at an appropriate angle and 2–3 cm above the agitator to ensure that the particles can easily flow through the probe window. The laser beam is emitted along the length of the probe tube through an array of optics and focused onto the sapphire window. The optical instrument rotates at a fixed speed (typically 2 m/s) so that the spot quickly scans the entire particle flowing through the window, as shown, and as the focused beam scans the entire particle system, individual particles or particle structures backscatter the laser beam to the detector. By detecting, counting, and multiplying the duration of each pulse by the scanning velocity of these unique pulses of backscattered light, the distance across each particle can be calculated. The distance between two particles is defined as the chord length and is the basic particle measurement distance related to particle size. Thousands of particles are typically counted and measured per second, allowing for accurate and highly sensitive real-time reporting of chord length distribution. The reaction is carried out in a flask, the reaction device is shown in Figure 2C, and the reaction conditions are consistent with the hydrogen production experiment.

2.5 Characterization

The functional groups and morphology of 25 μm aluminum powder were analyzed by FT-IR (IRAFFINITY-1) and SEM (TESCAN MIRA LMS) before reaction and after reaction for 2 h, 4 h, 6 h, 10 h and 12 h at 65°C, shown in Figure 2D.

3 Results and discussion

3.1 The initial exothermic of Al-water reaction

Figure 3 illustrates the heat flow curves of the Al-water reaction of two particle sizes under three heating rates, and Table 2 summarizes the initial exothermic temperature, peak temperature. The results of the experiment indicate that in the reaction process of aluminum and water, regardless of particle size, the heat release peak and peak temperature move backward gradually with the increase of heating rate. At the same heating rate, the initial exothermic temperature and peak temperature of reaction between sample 1 and water are lower than sample 2 in Figure 3 and Table 2. The initial exothermic temperature of reaction between sample 1 and water is about 170°C lower than that of reaction between sample 2 and water.

The temperature curves of the reaction system of the two aluminum powders and water under adiabatic conditions as a function of time are shown in Figure 4. It can be seen from Figure 4 that there is a period of heat release in the reaction between the two aluminum powders and water in the range of 30°C–350°C. Because sample 1 is easier to react with water, and its

10.3389/fenrg.2024.1441155

TABLE 2 The exothermic behavior of the Al-water reaction.

Sample	Heating rate (K/min)	T_{onset} (°C)	T_{peak} (°C)
3 μm Al + H_2O	5	74.9	80.7
	7.5	85.5	91.4
	10	86.6	93.4
25 μm Al + H_2O	5	248.0	261.6
	7.5	249.1	265.3
	10	260.7	277.2

heat release begins at 164 min, at this time the temperature is 51.9°C, while the reaction between sample 2 and water starts at 287 min. The temperature at which heat is released is 63.8°C.

3.2 Hydrogen production by the Al-water reaction

Experiments to produce hydrogen via the Al-water reaction are terminated at the end of each experiment when the reaction rate approaches zero, and it is not practical to continue the experiment until the Al-H_2O reaction is completely shut down. Therefore, the hydrogen production in the experiment will be slightly lower than the theoretical value. Under standard conditions, 1 g of aluminum reacts with water to produce about 1249 mL of hydrogen.

Figure 5A illustrate the hydrogen generation rate and hydrogen production with time during the reaction of sample 1 and water at 45°C–85°C. In the reaction process, the hydrogen generation rate reached the peak at the initial stage (2000–7000 s) of the reaction and began to decrease gradually. Meanwhile, hydrogen gas was accumulating continuously. When the reaction temperature increases, the time to reach the maximum reaction rate is shortened and the Al-H_2O reaction rate increases sharply. The temperature increased from 45°C to 85°C, and the maximum reaction rate increased from 0.18 mL•s^{-1}•g^{-1}–2.10 mL•s^{-1}•g^{-1}. The increase in temperature has a significant impact on the hydrogen production rate of the reaction of sample 1 with water, and the hydrogen production rate accelerates significantly with the increase of temperature, the maximum hydrogen production rate increases, and the time to reach the maximum hydrogen production rate is shortened, which has little effect on the hydrogen production rate.

As well as in the process of reacting sample 2 and water, as the temperature increases, its maximum reaction rate increases, and the hydrogen production rate is also increasing significantly, as shown in Figure 5B, because the temperature increase can make more molecules in the excited state, accelerating the water molecules into the aluminum particles, thereby promoting the reaction. The temperature increased from 45°C to 85°C, and the maximum reaction rate increased from 0.15 mL•s^{-1}•g^{-1} to 0.91 mL•s^{-1}•g^{-1}. It shows that the hydrogen production of sample 2 reacting with water is more affected by temperature. The increase in temperature not only has an impact on the hydrogen generation rate of the reaction of sample 2 with water, but also has a significant impact on the hydrogen production rate, and the maximum hydrogen generation rate is accelerated by the temperature increase, and the hydrogen generation rate is significantly increased. However, the overall hydrogen generation rate of sample 2 with water reaction is low, which may be related to the reaction time during the experiment.

Table 3 shows that the reaction of sample 1 with water was above 90% at 45°C–85°C, while the hydrogen production of sample 2 and water increased with increasing temperature, and the hydrogen generation of sample 2 with water was lower than that of sample 1 at the same temperature. However, the gap between the two decreased from 61% to 19% with the increase of temperature. The maximum hydrogen generation rate of aluminum powder with water increases with temperature. The difference between the maximum hydrogen generation rate and that of the sample

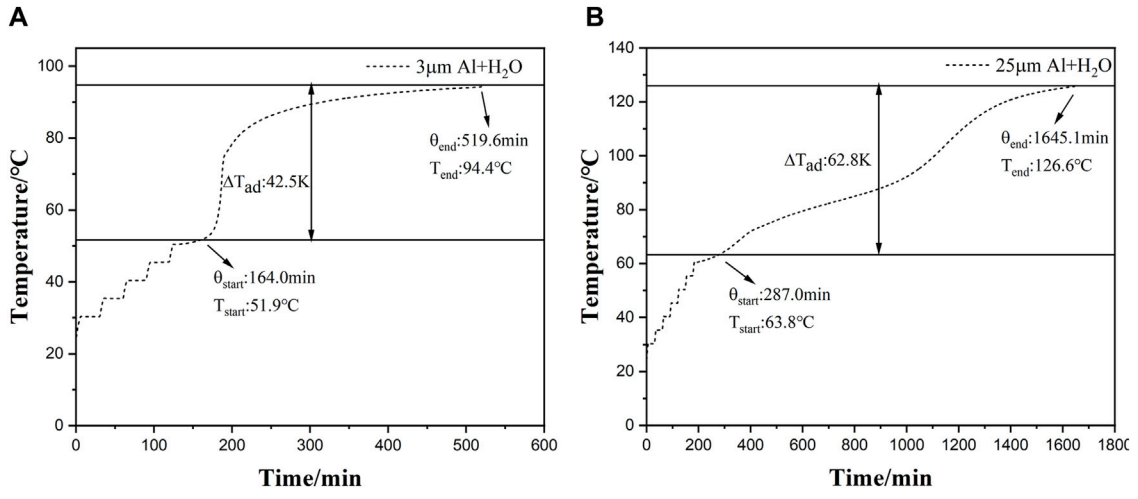

FIGURE 4
(A, B) Temperature change curves of the reaction of two aluminum powders with water against time under adiabatic conditions.

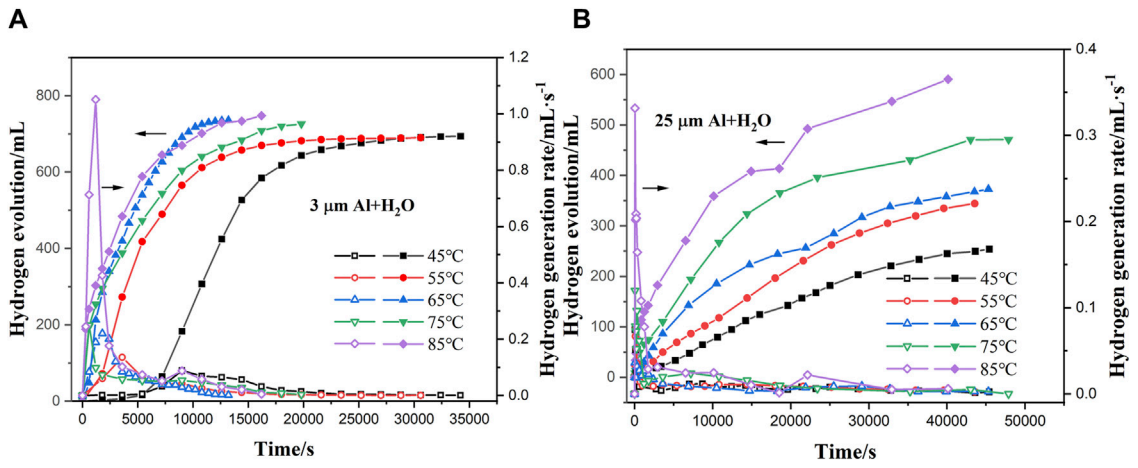

FIGURE 5
(A, B) Hydrogen evolution and hydrogen generation rates of the reaction of two aluminium powders with water over a temperature range ranging from 45°C to 85°C.

TABLE 3 Hydrogen production data from the Al-water reaction.

Partical size (μm)	Reaction temperature (°C)	Maximum hydrogen generation rate (mL/(s•g))	Hydrogen production (mL/g)	Hydrogen production rate (%)	Time to reach the maximum reaction rate (min)
3	45	0.18	1388	95	150
	55	0.27	1384	92	60
	65	0.44	1472	95	20
	75	1.20	1420	90	7
	85	2.10	1495	91	3
25	45	0.15	507.94	34	2
	55	0.15	688.28	45	3
	65	0.73	744.48	48	1
	75	0.33	941.6	59	0.5
	85	0.91	1181.08	72	0.5

1 was not obvious in the range of 45°C–65°C. The maximum hydrogen generation rate of the sample 1 was significantly accelerated after the temperature was increased, which was larger than that of the sample 2.

As shown in Equations 1–3 in Table 1, At the beginning of the reaction, hydrogen is not produced, but aluminum reacts with water to form AlO, AlH_3 and H., The product AlO and AlH_3 immediately react with water to produce hydrogen, and the hydrogen production speed is accelerated. Aluminum can also react directly with water to form hydrogen with hydroxides of different aluminum, as shown in Equation 4, 6, and 7 in Table 1. Finally, Al $(OH)_3$ is quickly consumed and continues to react with AlH_3 to form hydrogen, as shown in Equation 9.

For solid-liquid reactions, the contact area is an important factor affecting the reaction rate. The results of different particle sizes of aluminum powder at the same temperature show that the maximum hydrogen production rate of small particle size aluminum powder is higher than that of large particle size aluminum powder, and the greater the gap with the increase of temperature. Al powders of different particle sizes have different specific surface areas, and generally the larger the particle size of Al powders, the smaller the specific surface area. When the amount of pure Al powder participating in the reaction is constant, the larger the Al particle size, the smaller the total area in contact with water during the reaction, so the reaction rate is smaller. In addition, stirring is also a factor affecting the reaction rate. As stirring was carried out during the reaction in this experiment at a stirring rate of 220 r/min, stirring dispersed aluminum powder particles and increased the contact area with water molecules, thus speeding up the reaction between aluminum and water, and eliminating the influence of induction time on the reaction. Therefore, it can be seen from Figure 5 that hydrogen production basically occurred from the beginning of the reaction. However, Wang et al. (Guo et al., 2024)

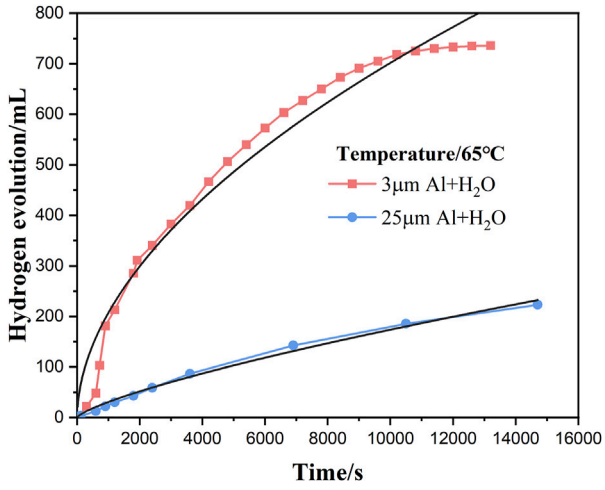

FIGURE 6
The fitting equation of time and hydrogen production of two particle sizes aluminum powders reacted with water at 65°C.

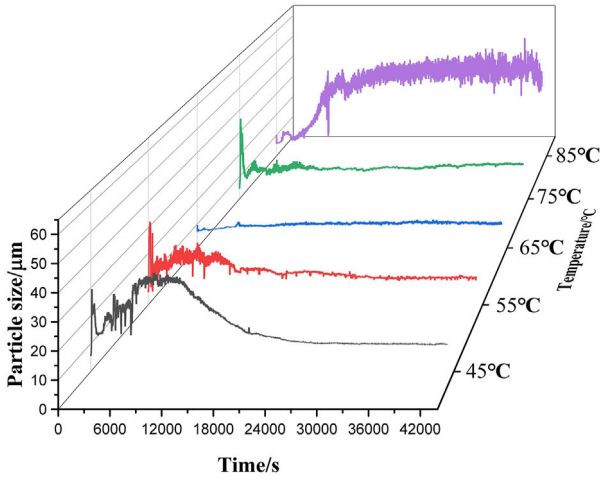

FIGURE 8
Particle size variation of 25 μm aluminum powder reacting with waterover a temperature range ranging from 45°C to 85°C.

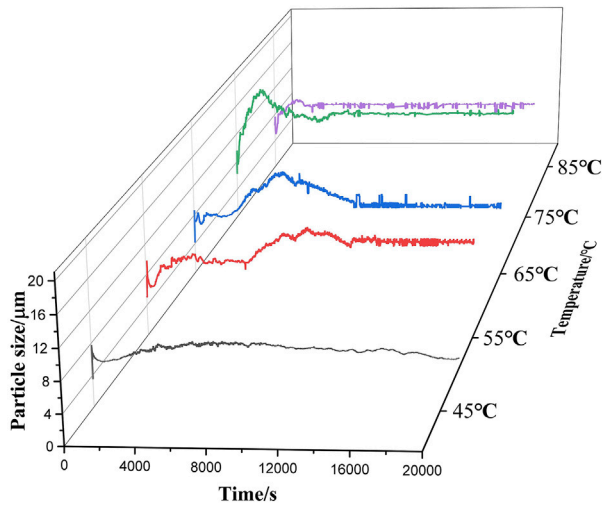

FIGURE 7
Particle size variation of 3 μm aluminum powder reacting with water over a temperature range ranging from 45°C to 85°C.

studied the Al-water reaction at 65°C–85°C without agitation, and the result was that hydrogen production occurred about 20–298 min after the reaction began. In this way, the speed of hydrogen production is solved and the safety hazard caused by local thermal runaway of reaction is solved.

Figure 6 shows the fitting equations for the reaction time and hydrogen production of aluminum powder with water of two particle sizes at 65°C. It can be seen from the figure that the relationship between time and hydrogen yield, and the linear fitting results are as follows:

$$V_{d_p} = \mathrm{a}t^b \begin{cases} a=5.34, b=0.53, d_p=3\mu m \\ a=0.17, b=0.75, d_p=25\mu m \end{cases} \quad (1)$$

3.3 *In-situ* analysis of particle size change in Al-water reaction

Figure 7 shows the particle size variation of sample 1 reacting with water at five temperatures ranging from 45°C to 85°C. The particle size of aluminum powder first increases to 13.16 μm and then decreases to 11 μm, and the particle size increases by 189% before and after the reaction. A similar trend was observed in Figure 8, which is the particle size variation of the reaction of sample 2 and water at 45°C–85°C, but the particle size of sample 2 increased to 34.86 μm and then decreased to 16.78 μm at 5 temperatures, and the particle size decreased by 29% before and after the reaction.

It can be seen that in the reaction process of sample 1 and water, the phases with the largest particle size are all at the peak stage of gas production rate in Figure 5A and Figure 7, while in the reaction process of sample 2 and water, the phases with the largest particle size are all after the peak stage of gas production rate in Figure 5B and Figure 8. Therefore, for sample 1, the increase of particle size during the reaction is conducive to the reaction to generate more hydrogen, while for sample 2, the increase of particle size will hinder the reaction, resulting in incomplete reaction and low hydrogen production rate when it reacts with water. When two aluminum particles with different particle sizes react with water at 65°C, online particle size real-time detection shows that the final products of the reaction between the two samples and water are stable at 9.76 μm and 9.78 μm, respectively, which are very similar. It might have relationship with the reaction conditions, like temperature. Because the Al-water reaction is greatly affected by temperature, the substances generated are not the same under different temperature conditions.

The initial particle size of aluminum powder differed between the two experimental groups, however the particle size test of the final product showed similar results. It can be observed that there are different stages in the reaction process of aluminum powder with

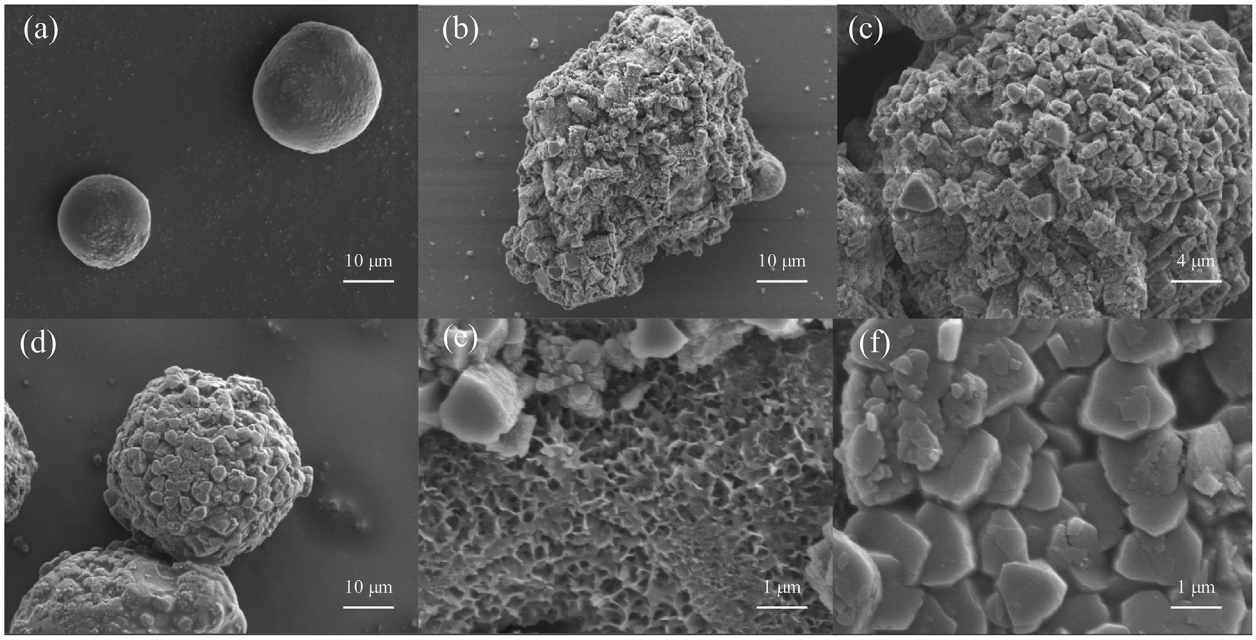

FIGURE 9
SEM images of the morphological variations of the product layer on top of the particles at different intervals of time were obtained: **(A)** initial aluminium powder; **(B)** 2 h after the start of the experiment; **(C)** 4 h after the start of the experiment; **(D)** 6 h after the start of the experiment; **(E)** 10 h after the start of the experiment; **(F)** at the end of the experiment.

water under the same conditions, which is also related to the difficulty of the reaction between aluminum powder and water, manifested by different reaction durations. Aluminum powder with smaller particle sizes reacts with water at a faster rate and undergoes the entire stage of surface reaction in a shorter time.

Hydrogen production from Al-water reaction is a complex process, in which the hydration reaction of passive film, condensation reaction between hydration layer and Al, the formation and growth of H_2 bubbles at Al/hydration layer interface until the break of hydration layer, and the direct reaction between H_2O and inner Al occurred in succession (Gai and Deng, 2024). Based on the SEM scanning electron microscopy images of the surface layer of intermediate products of particles at different reaction stages in Figure 9, it is shown that the morphology of the solid phase products generated during the aluminum water reaction process has undergone significant changes. As the reaction hydrogen production continues for 2 hours, the smooth particle surface becomes rougher than the original state of aluminum powder in Figures 9A, B. The solid products that react with water have obvious small area adhesion. After the reaction, the overall shape of the solid phase product changed significantly, but there were still spherical particles. Most of the solid products after reaction have relatively independent boundaries and regular shapes, and there is a large agglomeration phenomenon between particles, as shown in Figures 9C, D. Some small particles that remain spherical are completely attached to the surface of large bonded solid products, which corresponds to the increasing trend of particle size in Figures 7, 8. Subsequently, with the large-scale aggregation of solid phase products and particle aggregation, the subsequent development of the aluminum water reaction will be inhibited, and with the gradual generation of hydrogen gas, there will be a compressive stress effect between the gas and the oxide shell. The water molecules spread further inward, and the resulting hydroxide is a porous structure in Figure 9E. Hydrogen escapes through gaps in the hydroxide layer, while water makes further contact with the aluminum core. As the reaction continued to form a compact aluminum hydroxide in Figure 9F. Figure 9D shows that the particle size is significantly smaller than the morphology in Figure 9B at the same magnification. The initial reaction between aluminum particles with smaller particle sizes and water results in faster particle size development. The subsequent reaction process is hindered by various effects such as mass and subsequent aggregation.

When an oxide film is formed on the surface of the metal, stress occurs in the oxide film, which is caused by the volume ratio of the metal and oxide to expand or contract, corresponding to the compressive stress or tensile stress that occurs in the oxide film. The volume ratio of this metal and oxide is called Pilling-Bedworth ratio, referred to as PB ratio (Zhu, 1989), the aluminum surface to generate AlOOH volume and oxidation consumed matrix Al volume ratio is greater than 1 (calculated PB ratio is about 2.48), this stress is compressive stress, at the beginning, because the AlOOH layer thin plastic deformation is easy, can make the stress tend to ease, but with the water molecules step by step, the AlOOH layer thickens, the outermost AlOOH reacts with water to form $Al(OH)_3$. Plastic deformation becomes gradually difficult, and the internal stress cannot be alleviated, and finally the oxide film is ruptured or falling off.

TABLE 4 Common kinetic reaction mechanism functions.

Order of reaction	The differential form g(α)	The integral form G(α)
1/2	$2(1-\alpha)[-\ln(1-\alpha)]^{\frac{1}{2}}$	$[-\ln(1-\alpha)]^{\frac{1}{2}}$
1	$1-\alpha$	$-\ln(1-\alpha)$
2	$(1-\alpha)^2$	$\frac{1}{(1-\alpha)}$
3	$\frac{1}{2}(1-\alpha)^3$	$\left[\frac{1}{(1-\alpha)}\right]^2$

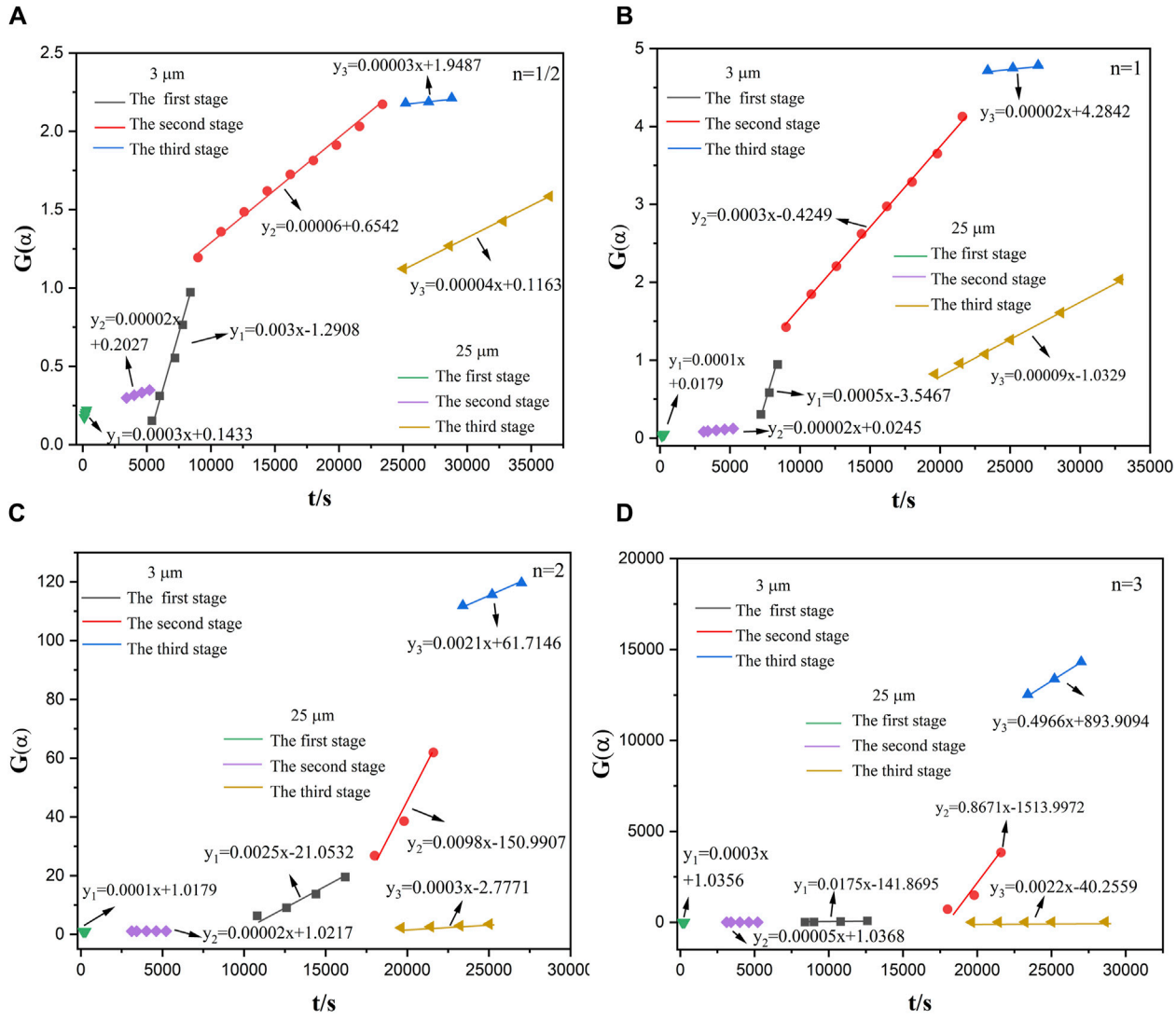

FIGURE 10
(A–D) Kinetic mechanism function fitting diagram of aluminum-water reaction at 45°C.

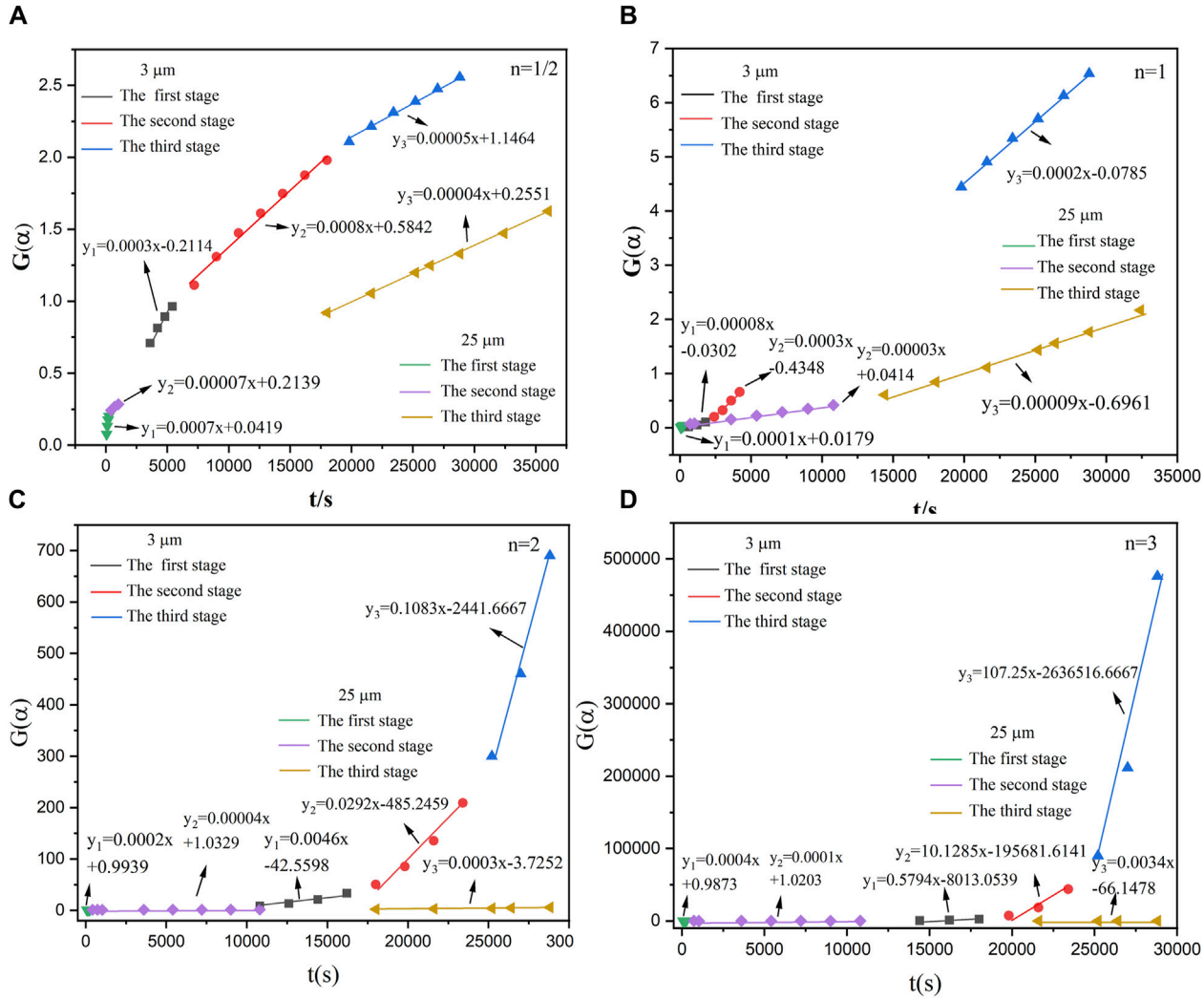

FIGURE 11
(A–D) Kinetic mechanism function fitting diagram of aluminum-water reaction at 55°C.

3.4 Analysis of Al-water reaction mechanism and kinetics

The kinetic calculation of the Al-water reaction was performed, and the kinetic equation was Arrhenius equation.

The kinetic equations are expressed as follows.

$$\frac{d\alpha}{dt} = kg(\alpha) = k(1-\alpha)^{\frac{1}{2}} = Ae^{-\frac{E_a}{RT}}(1-\alpha)^{\frac{1}{2}} \quad (2)$$

$$g(\alpha) = 2(1-\alpha)[-\ln(1-\alpha)]^{\frac{1}{2}} \quad (3)$$

where $g(\alpha) = (1-\alpha)^{1/2}$ is the reaction mechanism function; α is the reaction conversion rate (%).

The kinetic mechanism function G(α) in integral form as follows.

$$G(\alpha) = \int_0^t Ae^{-\frac{E_a}{RT}}dt = kt \quad (4)$$

The mechanism functions of differential and integral forms for different reaction orders are shown in Table 4.

According to Figure 5, the relationship between the conversion rate (α) and the time (t) of the reaction between aluminum powder and water of two particle sizes was calculated. The aluminum-water reaction could be divided into three stages. Figures 10–14 show the fitted reaction kinetic mechanism functions at 45°C–85°C, respectively. The aluminum-water reaction could be divided into three stages. The fitting results of kinetic mechanism functions at different temperatures and levels are shown in Supplementary Appendix A. For the reaction of 3 μm aluminum powder with water, in the first stage, the best fit was achieved at a reaction level of 1/2. In the second stage, the best fitting effect was obtained when the reaction order was 1. In the third stage, the best fit was achieved at a reaction level of 1/2. The kinetic parameters established for the three-reaction stage were $E_{a,1}$ = 15.20 kJ•mol^{-1}, $E_{a,2}$ = 11.55 kJ•mol^{-1}, $E_{a,3}$ = 45.46 kJ•mol^{-1}.

For the reaction of 25 μm aluminum powder with water, in the first stage, the best fit was achieved at a reaction level of 3. In the second stage, the best fitting effect was obtained when the reaction order was 1/2. In the third stage, the best fit was achieved at a reaction level of 1. The kinetic parameters established for the three-

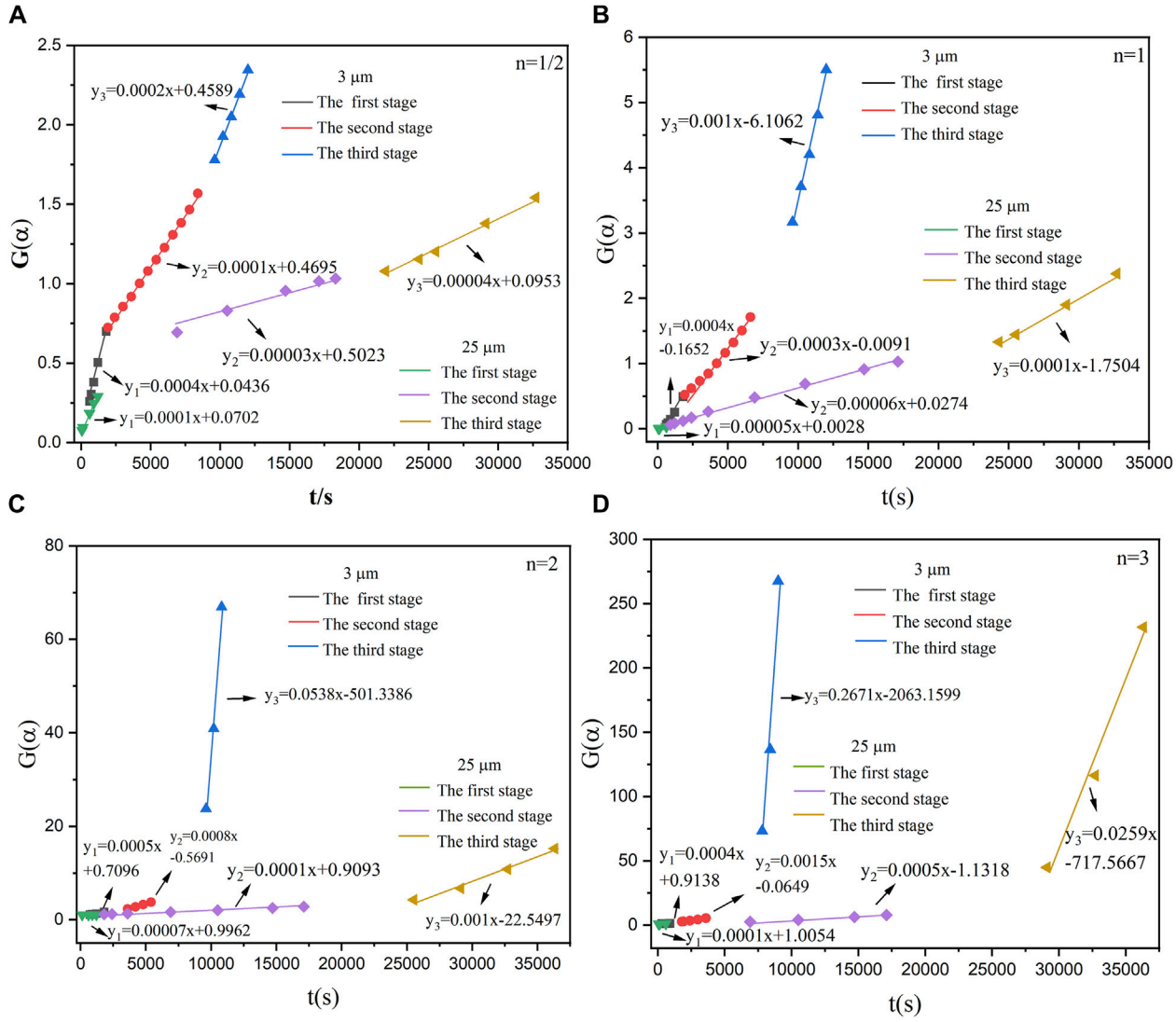

FIGURE 12
(A–D) Kinetic mechanism function fitting diagram of aluminum-water reaction at 65°C.

reaction stage were $E_{a,\,1}$ = 43.67 kJ•mol^{-1}, $E_{a,\,2}$ = 12.09 kJ•mol^{-1}, $E_{a,\,3}$ = 13.24 kJ•mol^{-1}.

Studies have tested the reaction of 25 μm aluminum powder with water at 90°C–200°C, and used the Arrhenius formula to calculate the activation energy of the Al-water reaction (Gao et al., 2023), they divided the Al-water reaction into two stages at different temperatures. The results are $E_{a,1}$ = 27.03 kJ•mol^{-1}, $E_{a,2}$ = 40.90 kJ•mol^{-1}. As can be seen from Table 5, the total activation energy of the reaction of 25 μm aluminum powder with water in this experiment is similar to the results of Gao et al. (Gao et al., 2023). In the first stage, the activation energy is high, which may be due to the effect of temperature on the Al-water reaction. The higher the activation energy is, the more sensitive the reaction rate is to temperature, and the higher the temperature is, the faster the reaction rate is, resulting in the lower activation energy in the second stage. The activation energy of each stage of the reaction between sample 1 and water is smaller than that of sample 2.

For the reaction of pure aluminum powder with water at normal pressure, the possible mechanism leading to changes in activation energy is particle size distribution (Nikolaevich et al., 2014). The particle size distribution of different aluminum powders is different. Generally, the width of the aluminum particle size distribution increases with the increase of its average particle size. Figure 1 shows the particle size distribution of two kinds of aluminum powder, of which the particle size distribution width of sample 2 (4.6–139.2 μm) is significantly greater than the width of sample 1 (0.7–13.4 μm).

4 Conclusions

To investigate the heterogeneous reaction between pure aluminium powder and water, a series of isothermal experiments were conducted within the temperature range of 45°C–85°C. The focus was on examining the morphological evolution and particle

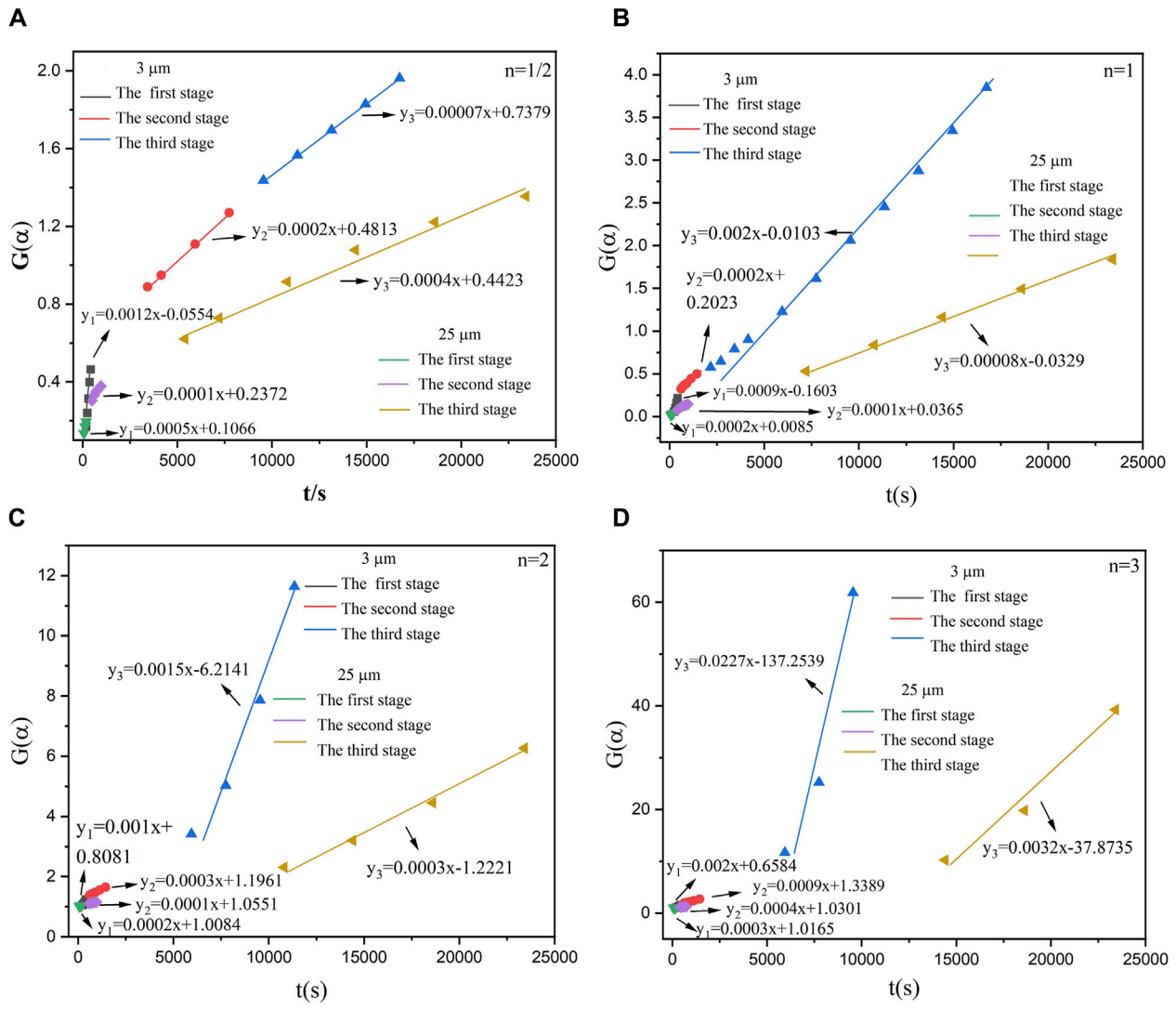

FIGURE 13
(A–D) Kinetic mechanism function fitting diagram of aluminum-water reaction at 75°C.

size variations of aluminum particles during the reaction process. Furthermore, an in-depth analysis was performed to elucidate the kinetic mechanism underlying the Al-water reaction at temperatures ranging from 45°C to 85°C. The conclusions draw from this work are as follows.

(1) Under identical conditions, the initial heat release temperature and peak temperature of the reaction between 3 μm aluminum powder and water exhibit a reduction of approximately 170°C compared to that observed with 25 μm aluminum powder. Under the adiabatic condition, the initial heat release temperature and the reaction peak temperature of 3 μm aluminum powder with water are about 11.9°C lower than 25 μm aluminum powder.

(2) In the process of Al-water reaction, the hydrogen production of 3 μm aluminum powder with water exceeds 90% within the temperature range of 45°C–85°C. Conversely, the hydrogen production from 25 μm aluminum powder increases with rising temperature; however, it remains lower than that achieved by using 3 μm aluminum powder at equivalent temperatures. However, the gap between the two decrease from 61% to 19% with the increase of temperature. With the temperature increases, the maximum hydrogen generation rate of the 3 μm aluminum powder is significantly accelerated, which was larger than that of the 25 μm aluminum powder, and the difference between the maximum hydrogen generation rate and that of the 25 μm aluminum powder increases from 0.01 $mL•s^{-1}$ to 0.59 $mL•s^{-1}$.

(3) During the Al-water reaction, there is an initial increase followed by a subsequent decrease in particle size. Specifically, the particle size of 3 μm aluminum powder initially increases to 13.16 μm and then decreases to 11 μm, resulting in a 189% overall increase before and after the reaction. Conversely, for the larger particle size of 25 μm aluminum powder, it first increases to 34.86 μm and

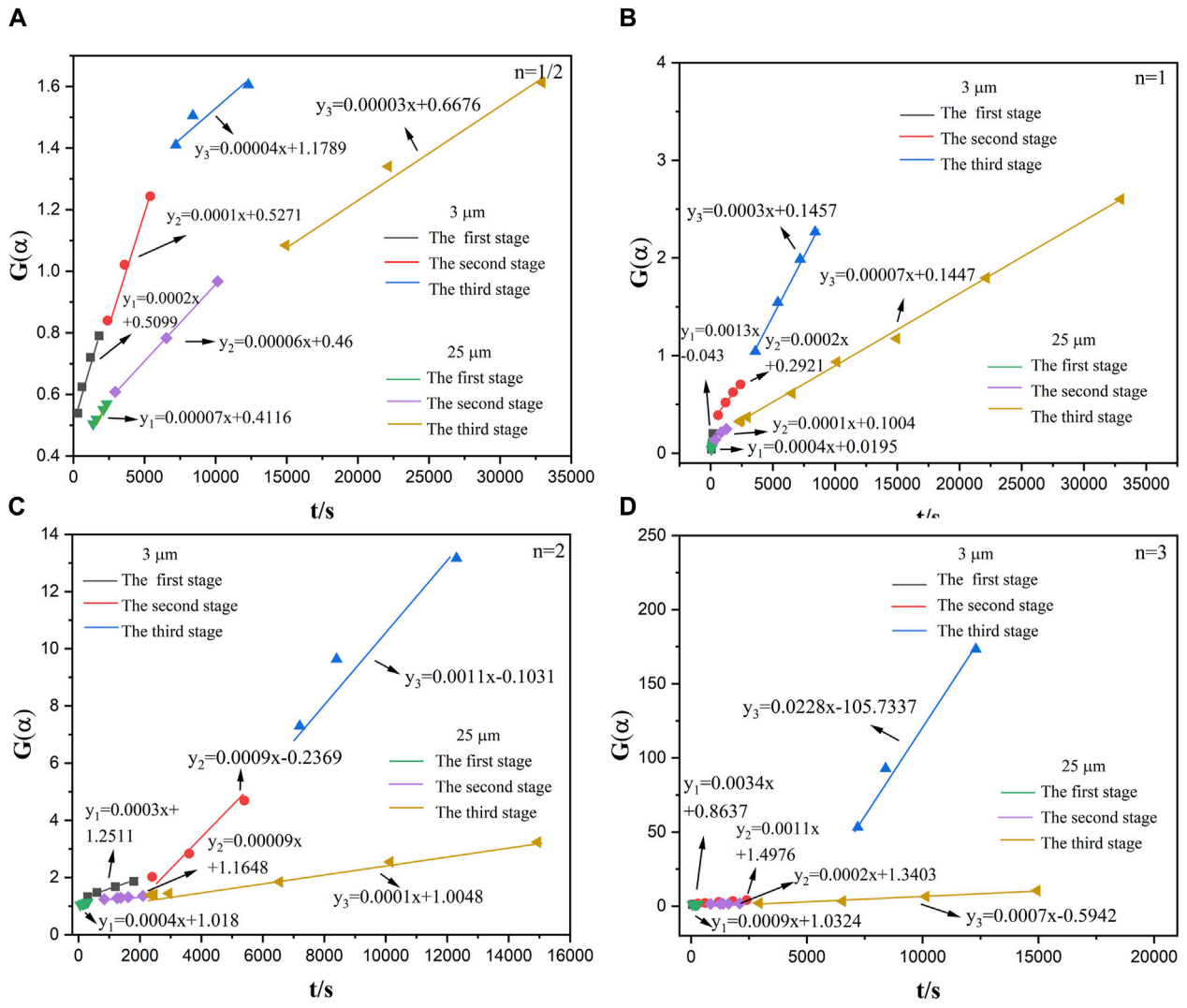

FIGURE 14
(A–D) Kinetic mechanism function fitting diagram of aluminum-water reaction at 85°C.

TABLE 5 Activation energy at each stage of the Al-water reaction.

Particle size (μm)	E_a (kJ/mol)			
	The first stage	The second stage	The third stage	$E_1+E_2+E_3$
3	15.20	11.55	18.71	45.46
25	43.67	12.90	13.24	69.81
25[a]	27.03	40.90	-	67.93

[a]Data from Ref. (Gao et al., 2023).

subsequently decreases to 16.78 μm at various temperatures, leading to a reduction of 29% in particle size before and after the reaction occurs. It is noteworthy that when smaller particles react with water, their increased size promotes the reaction; however, this trend is reversed for larger particles. Moreover, under identical conditions, large particles exhibit a more pronounced decreasing trend in terms of particle size compared to small particles until both sizes eventually converge.

(4) The Al water reaction at different temperatures can be broken down into four steps. The first three stages involve reaction kinetics, and the kinetic parameters of 3 μm aluminum powder at different reaction stages are $E_{a,\ 1}$ = 23.95 kJ•mol^{-1}, $E_{a,\ 2}$ = 9.58 kJ•mol^{-1}, $E_{a,\ 3}$ = 56.44 kJ•mol^{-1}. The kinetic parameters of 25 μm aluminum powder at different reaction stages are $E_{a,\ 1}$ = 25.99 kJ•mol^{-1}, $E_{a,\ 2}$ = 12.09 kJ•mol^{-1}, $E_{a,\ 3}$ = 13.24 kJ•mol^{-1}. The reaction rate is initially controlled by surface chemical reactions. As the reaction progresses, the outer layer of aluminum hydroxide gradually increases, water molecules are difficult to pass through, the reaction rate gradually decreases, and internal diffusion becomes the control step.

Data availability statement

The original contributions presented in the study are included in the article/Supplementary Material, further inquiries can be directed to the corresponding author.

Author contributions

XZ: Writing–review and editing. LW: Supervision, Writing–original draft, Writing–review and editing. GT: Investigation, Writing–review and editing. RG: Writing–review and editing. JF: Writing–review and editing. JZ: Writing–review and editing. HM: Resources, Writing–review and editing.

Funding

The author(s) declare that no financial support was received for the research, authorship, and/or publication of this article.

Conflict of interest

The authors declare that the research was conducted in the absence of any commercial or financial relationships that could be construed as a potential conflict of interest.

Publisher's note

All claims expressed in this article are solely those of the authors and do not necessarily represent those of their affiliated organizations, or those of the publisher, the editors and the reviewers. Any product that may be evaluated in this article, or claim that may be made by its manufacturer, is not guaranteed or endorsed by the publisher.

Supplementary material

The Supplementary Material for this article can be found online at: https://www.frontiersin.org/articles/10.3389/fenrg.2024.1441155/full#supplementary-material

References

Alinejad, B., and Mahmoodi, K. (2009). A novel method for generating hydrogen by hydrolysis of highly activated aluminum nanoparticles in pure water. *Int. J. Hydrog. Energ.* 34, 7934–7938. doi:10.1016/j.ijhydene.2009.07.028

Aman, F. E., and Pradhan, S. K. (2022). Enhanced hydrogen evolution rate using Mg-Cu Galvanic Coupling electrodes and seawater electrolyte. *Mater. Lett.* 315, 131946. doi:10.1016/j.matlet.2022.131946

Ambaryan, G. N., Vlaskin, M. S., Dudoladov, A. O., Meshkov, E. A., Zhuk, A. Z., and Shkolnikov, E. I. (2016). Hydrogen generation by oxidation of coarse aluminum in low content alkali aqueous solution under intensive mixing. *Int. J. Hydrog. Energ.* 41, 17216–17224. doi:10.1016/j.ijhydene.2016.08.005

Bolt, A., Dincer, I., and Agelin-Chaab, M. (2020). Experimental study of hydrogen production process with aluminum and water. *Int. J. Hydrog. Energ.* 45, 14232–14244. doi:10.1016/j.ijhydene.2020.03.160

Brayek, M., Mohamed, A., Zied, D., Gueorgui, K., and Mohamed, S. (2019). Study of spark-ignition engine fueled with hydrogen produced by the reaction between aluminum and water in presence of KOH. *Arab. J. Sci. Eng.* 44, 695–705. doi:10.1007/s13369-018-3192-4

Chawla, K., Yadav, D. K., Bajpai, A., Kumar, S., Jain, I. P., and Lal, C. (2022). Effect of PdCl2 catalyst on the hydrogenation properties and sorption kinetics of Mg. *Sustain. Eng. Technol. Assess.* 51, 101981. doi:10.1016/j.seta.2022.101981

Chen, C., Tian, H., Fu, Z., Cui, X., Kong, F., Meng, G., et al. (2022). Pt NPs-loaded siloxene nanosheets for hydrogen co-evolutions from Zn-H2O fuel cells-powered water-splitting. *Appl. Catal. B* 304, 121008. doi:10.1016/j.apcatb.2021.121008

Chen, P., and Zhu, M. (2008). Recent progress in hydrogen storage. *Mater. Today* 11, 36–43. doi:10.1016/S1369-7021(08)70251-7

Chen, X. R., Wang, C. P., Liu, Y. H., Shen, Y. S., Liu, X., Yang, S., et al. (2020). Popcorn-like aluminum-based powders for instant low-temperature water vapor hydrogen generation. *Mater. Today Energ* 19, 100602. doi:10.1016/j.mtener.2020.100602

Chen, Y. K., Teng, H. T., Lee, T. Y., and Wang, H. W. (2014). Rapid hydrogen generation from aluminum–water system by adjusting water ratio to various aluminum/aluminum hydroxide. *Int. J. Energy Environ. Eng.* 5, 87. doi:10.1007/s40095-014-0087-3

Das, L. M. (1996). Hydrogen-oxygen reaction mechanism and its implication to hydrogen engine combustion. *Int. J. Hydrog. Energ.* 21, 703–715. doi:10.1016/0360-3199(95)00138-7

Dong, R. K., Mei, Z., Zhao, F. Q., Xu, S. Y., and Ju, X. H. (2019). Molecular dynamics simulation on the reaction of nano-aluminum with water: size and passivation effects. *RSC Adv.* 9, 41918–41926. doi:10.1039/C9RA08484C

El-Meligi, A. A. (2011). Hydrogen production by aluminum corrosion in hydrochloric acid and using inhibitors to control hydrogen evolution. *Int. J. Hydrogen Energy* 36, 10600–10607. doi:10.1016/j.ijhydene.2011.05.111

Fu, S. H., Lou, W. Z., Wang, H. J., Li, C. B., Chen, Z. H., and Zhang, Y. (2020). Evaluating the effects of aluminum dust concentration on explosions in a 20 L spherical vessel using ultrasonicsensors. *Powder Technol.* 367, 809–819. doi:10.1016/j.powtec.2020.02.015

Gai, W. Z., and Deng, Z. Y. (2024). Enhanced hydrogen production from Al-water reaction: strategies, performances, mechanisms and applications. *Renew. Energy* 226, 120397. doi:10.1016/j.renene.2024.120397

Gai, W. Z., Liu, W. H., Deng, Z. Y., and Zhou, J. G. (2012). Reaction of Al powder with water for hydrogen generation under ambient condition. *Int. J. Hydrog. Energ.* 37, 13132–13140. doi:10.1016/j.ijhydene.2012.04.025

Gao, X., Wang, C., Bai, W., Hou, Y., and Che, D. (2023). Experimental investigation of the catalyst-free reaction characteristics of micron aluminum powder with water at low and medium temperatures. *J. Energy Storage* 59, 106543. doi:10.1016/j.est.2022.106543

Godart, P., Fischman, J., Seto, K., and Hart, D. (2019). Hydrogen production from aluminum-water reactions subject to varied pressures and temperatures. *Int. J. Hydrog. Energ.* 44, 11448–11458. doi:10.1016/j.ijhydene.2019.03.140

Guo, X. H., Ma, G. W., Wang, X. Y., Gai, W. Z., and Deng, Z. Y. (2024). Al-water reaction generates metastable aluminum cluster ions and their use in advanced oxidation processes. *Sep. Purif. Technol.* 349, 127838. doi:10.1016/j.seppur.2024.127838

Huang, H. J., Tu, H. T., Xu, H. J., Shi, P. L., and Wang, D. H. (2023). Insight of external ultrasound on energy-production acceleration from renewable Al-water reaction in Al-based metallic materials. *Energ* 48, 20253–20263. doi:10.1016/j.ijhydene.2022.09.239

Huang, X. N., Gao, T., Pan, X. L., Wei, D., Lv, C. J., Qin, L. S., et al. (2013). A review: feasibility of hydrogen generation from the reaction between aluminum and water for fuel cell applications. *J. Power Sources* 229, 133–140. doi:10.1016/j.jpowsour.2012.12.016

Ilyukhina, A. V., Kravchenko, O. V., and Bulychev, B. M. (2017). Studies on microstructure of activated aluminum and its hydrogen generation properties in aluminum/water reaction. *J. Alloys Compd.* 690, 321–329. doi:10.1016/j.jallcom.2016.08.151

Jiang, H. P., Bi, M. S., Zhang, T. J., Shang, S., and Gao, W. (2021). A novel reactive P-containing composite with an ordered porous structure for suppressing nano-Al dust explosions. *Chem. Eng. J.* 416, 129156. doi:10.1016/j.cej.2021.129156

Kumar, D., and Muthukumar, K. (2020). An overview on activation of aluminium-water reaction for enhanced hydrogen production. *J. Alloys Compd.* 835, 155189. doi:10.1016/j.jallcom.2020.155189

Li, Y., Shi, Z., Chen, X., and Atrens, A. (2021). Anodic hydrogen evolution on Mg. *J. Magnes. Alloys* 9, 2049–2062. doi:10.1016/j.jma.2021.09.002

Milani, M., Montorsi, L., Storchi, G., Venturelli, M., Angeli, D., Leonforte, A., et al. (2020). Experimental and numerical analysis of a liquid aluminium injector for an Al-H2O based hydrogen production system. *Int. J. Thermofluids* 7-8, 100018–8. doi:10.1016/j.ijft.2020.100018

Nikolaevich, L. M. (2014). "Reaction of aluminum powders with liquid water and steam," in *Metal nanopowders: production, characterization, and energetic applications*. Editors A. Gromov and U. Teipel (Weinheim: Wiley-VCH Verlag GmbH and Co. KGaA). doi:10.1002/9783527680696.ch8

Parmuzina, A. V., and Kravchenko, O. V. (2008). Activation of aluminium metal to evolve hydrogen from water. *Int. J. Hydrog. Energ.* 33, 3073–3076. doi:10.1016/j.ijhydene.2008.02.025

Razavi-Tousi, S. S., and Szpunar, J. A. (2014). Mechanism of corrosion of activated aluminum particles by hot water. *Electrochim. Acta* 127, 95–105. doi:10.1016/j.electacta.2014.02.024

Saceleanu, F., Vuong, T. V., Master, E. R., and Wen, J. Z. (2019). Tunable kinetics of nanoaluminum and microaluminum powders reacting with water to produce hydrogen. *Int. J. Energy Res.* 43, er.4769–7396. doi:10.1002/er.4769

Shkolnikov, E. I., Zhuk, A. Z., and Vlaskin, M. S. (2011). Aluminum as energy carrier: feasibility analysis and current technologies overview. *Renew. Sustain. Energy Rev.* 15, 4611–4623. doi:10.1016/j.rser.2011.07.091

Soler, L., Candela, A. M., Macanas, J., Munoz, M., and Casado, J. (2009). *In situ* generation of hydrogen from water by aluminum corrosion in solutions of sodium aluminate. *J. Power Sources* 192, 21–26. doi:10.1016/j.jpowsour.2008.11.009

Tan, Y. H., Yang, H. T., Cheng, J. X., Hu, J. C., Tian, G. C., and Yu, X. H. (2022). Preparation of hydrogen from metals and water without CO2 emissions. *Int. J. Hydrog. Energ.* 47, 38134–38154. doi:10.1016/j.ijhydene.2022.09.002

Tang, W. Q., Yan, L. H., Li, K. Q., Juan, Y. F., Fu, C. P., and Zhang, J. (2022). A comparison study on aluminum-water reaction with different catalysts. *Today Commun.* 31, 103517. doi:10.1016/j.mtcomm.2022.103517

Tekade, S. P., Shende, D. Z., and Wasewar, K. L. (2018). Hydrogen generation in water splitting reaction using aluminum: effect of NaOH concentration and reaction modelling using SCM. *Int. J. Chem. React. Eng.* 16. doi:10.1515/ijcre-2017-0250

Trowell, K. A., Goroshin, S., Frost, D. L., and Bergthorson, J. M. (2020). Aluminum and its role as a recyclable, sustainable carrier of renewable energy. *Appl. Energ.* 275, 115112. doi:10.1016/j.apenergy.2020.115112

Wang, X., Li, G., and Eckhoff, R. K. (2021). Kinetics study of hydration reaction between aluminum powder and water based on an improved multi-stage shrinking core model. *Int. J. Hydrog. Energ.* 46, 33635–33655. doi:10.1016/j.ijhydene.2021.07.191

Wei, H., Si, J. C., Zeng, L. B., Lyu, S., Zhang, Z. G., Suo, Y., et al. (2022). Electrochemically exfoliated Ni-doped MoS2 nanosheets for highly efficient hydrogen evolution and Zn-H2O battery. *Chin. Chem. Lett.* 34, 107144. doi:10.1016/j.cclet.2022.01.037

Xiao, F., Guo, Y. P., Yang, R. J., and Li, J. M. (2019). Hydrogen generation from hydrolysis of activated magnesium/low-melting-point metals alloys. *Int. J. Hydrog. Energ.* 44, 1366–1373. doi:10.1016/j.ijhydene.2018.11.165

Yu, X. Z., Yan, X. Q., Yu, J. L., and Gao, W. (2022). Effects of aluminum particle size distributions on the explosion behaviors of hydrogen/aluminum dust hybrid mixtures. *Powder Technol.* 405, 117548. doi:10.1016/j.powtec.2022.117548

Zhang, J., Li, Z., Wu, Y., Guo, X., Ye, J., Yuan, B., et al. (2019). Recent advances on the thermal destabilization of Mg-based hydrogen storage materials. *RSC Adv.* 9, 408–428. doi:10.1039/C8RA05596C

Zhang, Y., Xu, K., Ge, J., and Liu, B. (2022a). Study on hydrogen evolution risk and suppression methods of Mg-Al/Mg-Zn alloy waste dust in wet dust collector. *Process Saf. Environ. Prot.* 163, 321–329. doi:10.1016/j.psep.2022.04.040

Zhang, Y. Y., Xu, K., Liu, B., and Wang, B. (2022b). Effects of different metal corrosion inhibitors on hydrogen suppression and film formation with Mg–Zn alloy dust in NaCl solutions. *Int. J. Hydrog. Energ.* 47, 29172–29183. doi:10.1016/j.ijhydene.2022.06.237

Zhu, R. Z. (1989). *Corrosion science of metal*. Beijing: Metallurgical Industry Press.

Ziebarth, J. T., Woodall, J. M., Kramer, R. A., and Choi, G. (2011). Liquid phase-enabled reaction of Al–Ga and Al–Ga–In–Sn alloys with water. *Int. J. Hydrog. Energ.* 36, 5271–5279. doi:10.1016/j.ijhydene.2011.01.127

10.3389/fenrg.2024.1441155

Nomenclature

$\mathbf{T_{onset}}$	Initial exothermic temperature (°C)
$\mathbf{T_{peak}}$	Peak temperature (°C)
ΔTad	Adiabatic temperature rise (K)
E	Activation energy (kJ/mol)
R	Gas constant (kJ/mol·K)